





Target dependence of postcollision interaction effects on fully differential ionization cross sectionsM. Dhital ¹, S. Bastola,¹ A. Silvus,¹ B. R. Lamichhane,¹ E. Ali ¹, M. F. Ciappina,² R. Lomsadze ³, A. Hasan ⁴,
D. H. Madison,¹ and M. Schulz¹¹*Department of Physics and LAMOR, Missouri University of Science & Technology, Rolla, Missouri 65409, USA*²*Institute of Physics of the ASCR, ELI-Beamlines, Na Slovance 2, 182 21 Prague, Czech Republic*³*Tbilisi State University, Tbilisi 0179, Georgia*⁴*Department of Physics, UAE University, P.O. Box 15551, Al Ain, Abu Dhabi, United Arab Emirates*

(Received 22 July 2019; published 16 September 2019)

We have measured and calculated fully differential cross sections (FDCS) for ionization of helium by 75-keV proton impact. Ejected electrons with a speed close to and above the projectile speed were investigated. This range of kinematics represents a largely unexplored regime. A high sensitivity of the FDCS to the details of the description of the few-body dynamics, reported earlier for ionization of H₂, was confirmed. A peak structure was found in an electron angular range between the regions where the so-called binary and recoil peaks are usually observed. The need for nonperturbative calculations using a two-center basis set is demonstrated.

DOI: [10.1103/PhysRevA.100.032707](https://doi.org/10.1103/PhysRevA.100.032707)**I. INTRODUCTION**

Ionization of atoms and molecules by ion impact has been studied extensively for several decades (for reviews see, e.g., [1–4]). Early experiments focused on measuring absolute total cross sections (see, e.g., [5–9]). Later, with the development of high-resolution electron spectrometers, double differential cross-section measurements became feasible (see, e.g., [10–12]). However, cross sections differential in projectile parameters were very challenging to measure because of the large mass of ions compared to electrons. Direct detection of fast, heavy projectiles with sufficient resolution was restricted to scattering angles larger than approximately 0.1 mrad and energy losses larger than approximately 100 eV [13,14]. However, for ionization from the target valence shell the largest contributions to the cross section often come from much smaller scattering angles (of the order of μ rad or even smaller) and energy losses (close to the target ionization potential). Until about 20 years ago projectile differential cross sections for valence-shell ionization, in the kinematic regime which mostly contributes to the total cross section, could only be measured for light-ion impact (see, e.g., [15]). Double differential measurements (as a function of scattering angle and energy loss) were further limited to relatively small projectile energies (see, e.g., [16]). Fully differential cross sections (FDCS) were only measured [4,17–21] after recoil-ion momentum spectroscopy was developed [22,23]. For fast heavy-ion impact this made possible measuring the momentum vectors of the ejected electron and the recoil ion in coincidence and to determine the scattered projectile momentum from the kinematic conservation laws.

So far, FDCS measurements were focused on electrons ejected with a speed much smaller than the projectile speed (see, e.g., [4,17–21]). Fully differential data for ejected electron speeds close to the projectile speed were only reported for 75-keV $p + \text{H}_2$ collisions [24], and such data for electrons considerably faster than the projectile as far as we know

have not been reported yet. The projectile–electron velocity-matching regime has attracted considerable interest (see, e.g., [10,16,25,26]) because here a specific higher-order mechanism, known as postcollision interaction (PCI), plays a particularly important role, especially for low- and intermediate-energy projectiles. In this process, the projectile interacts at least twice with the active electron. In the primary interaction the projectile transfers sufficient energy to the electron for the latter to be lifted to the continuum, and subsequently the two particles interact with each other for a second time, in which they attract each other toward the initial projectile beam axis and to similar velocities. Furthermore, because of momentum conservation, an interaction between the residual target ion and either the projectile or the active electron needs to be involved in PCI [27]. As a result, the leading-order interaction sequences leading to PCI are $V_{pe}-V_{te}-V_{pe}$ and $V_{pe}-V_{pt}-V_{pe}$, where the subscripts p , t , and e refer to projectile, target ion, and electron, respectively. As pointed out by Sarkadi *et al.* [28] PCI is therefore a two-center process.

One important manifestation of the focusing due to PCI predicted by theory [29,30] is a strong peak structure in the fully differential electron angular distribution in the velocity-matching regime occurring in the forward direction. This forward peak was recently confirmed experimentally for the case of an H₂ target [24]. Nevertheless, large discrepancies between experiment and theory and between two conceptually very similar theoretical models were found. In contrast, for electron energies well below the velocity-matching regime discrepancies between experiment and theory are much smaller and various theoretical models are usually in reasonable agreement with each other [31,32]. This illustrates that, in the velocity-matching regime, the FDCS are very sensitive to the details of the few-body dynamics. Therefore, this regime is particularly important to test theoretical models.

Further signatures of PCI, which are not fully understood, were found in double differential cross sections (DDCS) as a function of scattering angle, which were measured for a

broad range of ejected electron energies and for several target species [33]. For ejected electron energies below the velocity-matching regime focusing effects due to PCI appeared to become increasingly pronounced with increasing target ionization potential I , which is the expected and theoretically predicted trend [24]. However, at the velocity matching the trend was not clear. On the one hand, the width of the scattering angle dependence of the DDCS increased with increasing I , suggesting a decreasing focusing due to PCI. On the other hand, a broadening of the DDCS could be caused by another higher-order mechanism, involving the projectile-target nucleus (PT) interaction, but only a single projectile-electron interaction. Such a process should become increasingly important with increasing I . It is thus possible that PCI increases with increasing I even at the velocity matching, but that it is masked by the higher-order mechanism involving the PT interaction. The results of [24,33] show that our understanding of the few-body dynamics in this regime is much less complete than it is for electron energies well below the velocity-matching regime.

In this paper we present measured FDCS for ionization in 75-keV $p + \text{He}$ collisions. Two main goals were pursued in this project: First, we wanted to investigate the target dependence of PCI effects on the FDCS by comparing data for a target with a relatively large I (24.6 eV for He) to previously reported data for a target with a relatively small I (15.4 eV for H_2). Second, we wanted to study the role of PCI for ejected electron energies well above the velocity-matching regime. We will show that a clear dependence of PCI effects on the target could not be identified in the electron angular distribution of the FDCS; however, fully differential electron energy spectra show a stronger role of PCI for He compared to H_2 at large projectile scattering angles. Furthermore, PCI effects remain surprisingly strong at electron energies well above the velocity-matching regime.

II. EXPERIMENTAL SETUP

The experiment was performed at the ion accelerator of the Missouri University of Science & Technology. The setup is identical to the one used previously to study ionization of H_2 [24]. A proton beam was generated with a hot cathode ion source and extracted at an energy of 5 keV and then accelerated to 75 keV. The beam, propagating in the z direction, was collimated by a pair of slits with a width of 150 μm placed at a distance of 50 cm from the target region. With a projectile de Broglie wavelength of 2×10^{-3} a.u. this slit geometry corresponds to a transverse coherence length of about 3.5 a.u. [34]. After passing through the target region, the projectiles were charge analyzed by a switching magnet. The projectiles which were not charge exchanged were decelerated by 70 keV, energy analyzed using an electrostatic parallel plate analyzer [35], and detected by a two-dimensional position-sensitive multichannel plate detector. From the position information and the energy loss ε the complete three-dimensional momentum vector was obtained in the data analysis. The resolution in ε was about 2.5 eV full width at half maximum (FWHM) and the scattering angle resolution 0.12 mrad FWHM.

In the collision chamber the projectile beam was crossed with a very cold helium beam ($T \approx 1\text{--}2$ K), propagating in the

y direction, from a supersonic jet. The recoil ions produced in the collision were extracted by a weak and uniform electric field of 6 V/cm and detected by a second two-dimensional position-sensitive detector, which was set in coincidence with the projectile detector. The coincidence time contains the time-of-flight information of the recoil ions from the collision region to the detector (the spread in the time of flight of the projectiles due to the energy loss is negligible), from which the momentum component in the direction of the extraction field (x direction) was determined. The y and z components of the recoil-ion momentum were extracted from the position information. The momentum resolution was about 0.15 a.u. FWHM for the x and z components and, due to the target temperature, 0.35 a.u. FWHM in the y direction.

The ejected electron momentum was deduced from momentum conservation as $\mathbf{p}_e = \mathbf{q} - \mathbf{p}_r$, where \mathbf{q} is the momentum transfer from the projectile to the target. The FDCS will be presented for electrons ejected with various fixed energies E_e into the scattering plane (spanned by the initial and final projectile momenta) and various fixed projectile scattering angles θ_p as a function of the electron emission angle θ_e . Since $E_e = \varepsilon - I$ ($I = 24.6$ eV = 0.904 a.u.), the electron energy resolution is the same as the resolution in ε . The angular resolution depends on θ_e itself and ranges from 8° in the forward direction to about 12° FWHM in the direction of \mathbf{q} , where the so-called binary peak (see Results and Discussion section) is usually observed.

III. THEORY

The data were compared to two different, but conceptually very similar distorted wave calculations. Our continuum distorted wave–eikonal initial state (CDW-EIS) model is a single active electron approach where we assume that in the final state the ejected electron moves in the combined Coulomb field of the incident ion and the residual target core. Partial screening of the active electron–target interaction due to the “passive” helium electron is modeled by means of a Hartree-Fock scheme. Distortion of the final electronic state by the projectile is represented by a pure Coulomb function, and by an eikonal phase in the entrance channel. In an extension of the CDW-EIS model, the projectile–residual target ion (PT) interaction is accounted for in terms of a pure Coulomb interaction between the projectile and the target core (CDW-EIS-PT model). This interaction is then included in the transition amplitude, by invoking the eikonal approximation, through its multiplication by a phase factor. For more details see [36].

Whereas the CDW-EIS-PT approach is a semiclassical approximation which treats the projectile motion as straight lines, the three-body distorted wave–eikonal initial state (3DW-EIS) model is a fully quantum-mechanical treatment. The incident projectile is treated as a plane wave with an eikonal phase approximating the initial state PT interaction. The final state wave function for the projectile is a Coulomb wave for a net charge of $+1$, so the final state PT interaction is approximated as the projectile moving in the field of the ion. The ejected electron wave function is a distorted wave which is a solution of the Schrödinger equation using a numerical potential whose radial dependence contains the screening

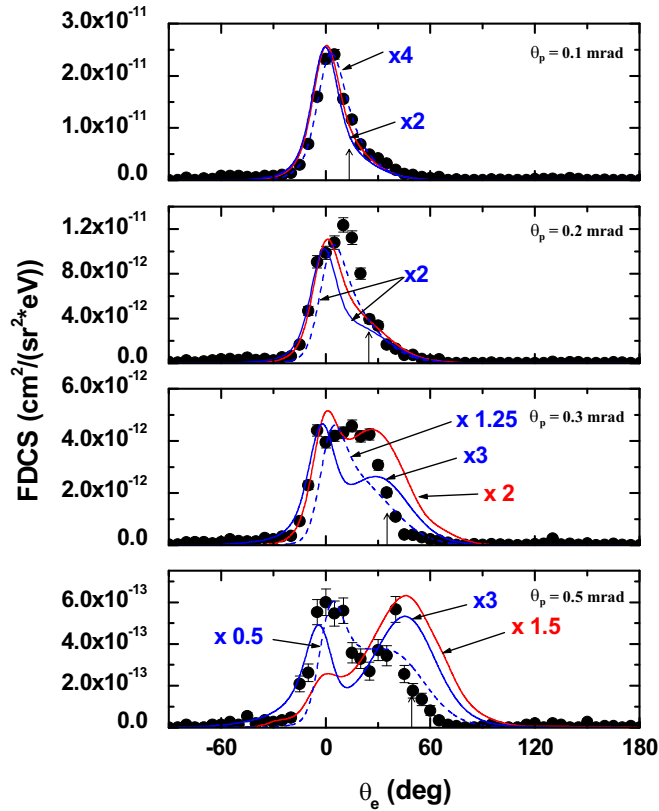


FIG. 1. Fully differential cross sections for electrons ejected into the scattering plane for a projectile energy loss of 62.5 eV as a function of electron ejection angle. The projectile scattering angles are indicated in the insets of each panel. The dashed blue curves represent the CDW-EIS calculations, the solid blue curves the CDW-EIS-PT calculations, and the red curves the 3DW-EIS calculations.

of the nucleus by the electron cloud. For small radii, this potential has a net charge equal to that of the nucleus. For increasing radii, the net charge reduces to that of the ion for radii larger than the size of the ion. For a more complete description, see [37] and references therein.

IV. RESULTS AND DISCUSSION

In Figs. 1–4 we present FDCS for energy losses of $\varepsilon = 62.5, 65.5, 68.5,$ and 85 eV (corresponding to electron to projectile speed ratios of 0.965, 1, 1.04, and 1.22, respectively), and for fixed scattering angles (from top to bottom panels) of $\theta_p = 0.1, 0.2, 0.3,$ and 0.5 mrad as a function of the polar electron emission angle θ_e . In each case electrons ejected into the scattering plane were selected; i.e., the azimuthal electron angle was fixed at $\varphi_e = 0^\circ \pm 5^\circ$. Here, $\theta_e = 0^\circ$ coincides with the initial projectile beam direction, $\theta_e = 90^\circ$ with the direction of the transverse component of \mathbf{q} , and $\theta_e = 270^\circ$ with the direction of the transverse component of $-\mathbf{q}$. The direction of \mathbf{q} [$\theta_q = \arctan(q_{1r}/q_z)$] is indicated by the arrow in each panel.

Qualitatively, the electron angular dependences of the FDCS are quite similar to those we recently reported for ionization of H_2 . For He, too, in most cases a strong forward peak is observed, which dominates the FDCS at small θ_p

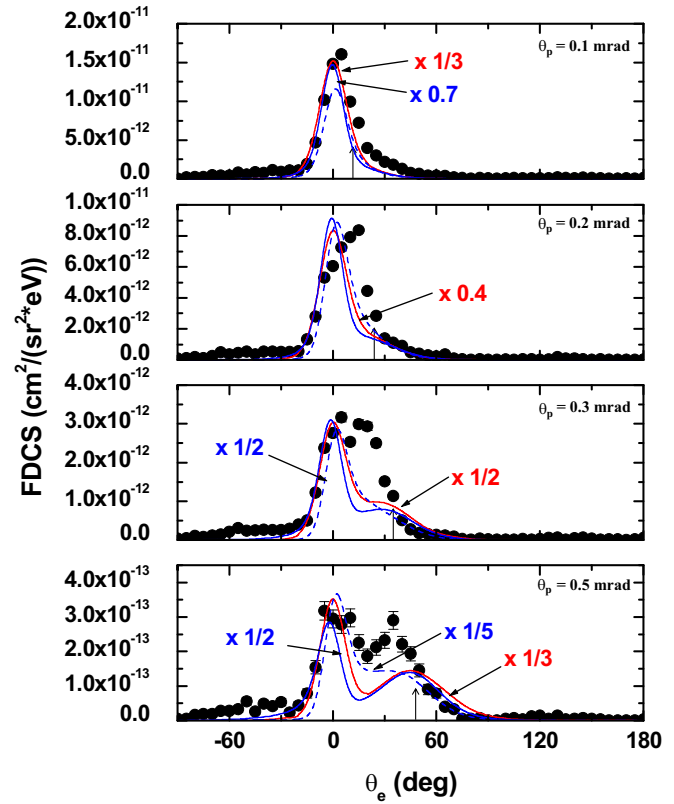


FIG. 2. Same as Fig. 1 for a projectile energy loss of 65.5 eV.

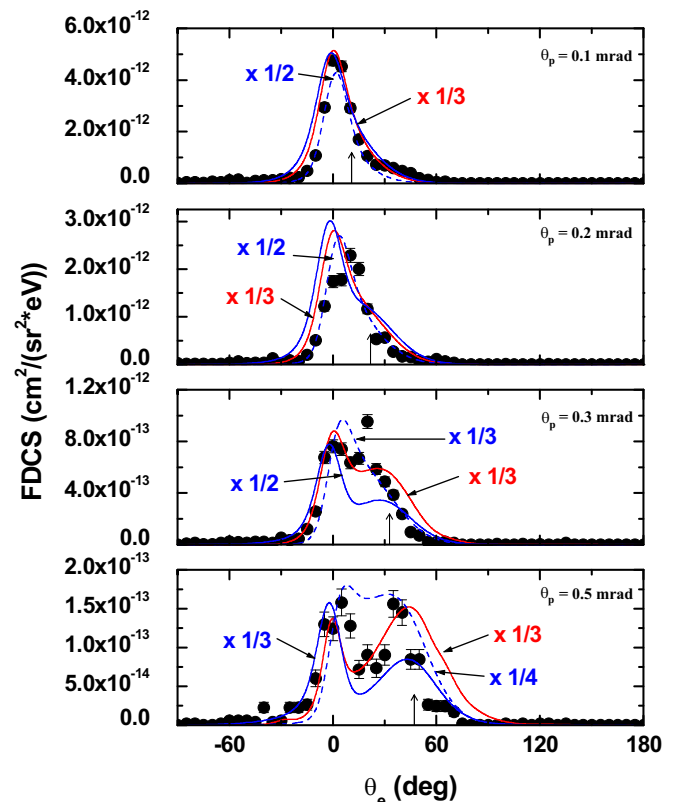


FIG. 3. Same as Fig. 1 for a projectile energy loss of 68.5 eV.

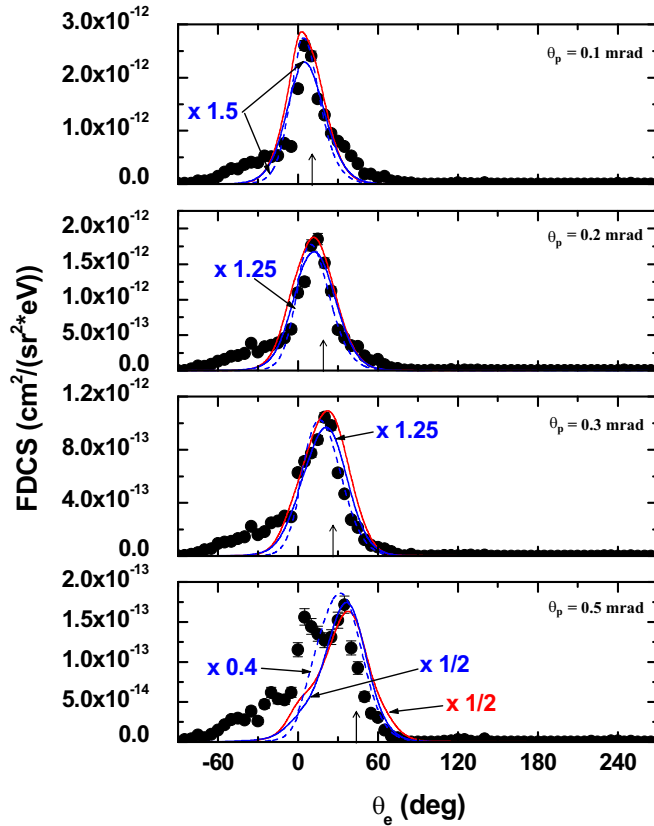


FIG. 4. Same as Fig. 1 for a projectile energy loss of 85 eV.

(except for $\varepsilon = 85$ eV). This structure is due to the mutual focusing of the projectile and the electron toward the beam axis caused by PCI. Furthermore, the binary peak, which is expected near the direction of \mathbf{q} , at small θ_p manifests itself in terms of a “shoulder” on the large-angle wing of the forward peak, and with increasing θ_p becomes increasingly visible as a separate peak structure. In a first-order approximation the binary peak can be described as being caused by a single interaction between the projectile and the electron, where the target nucleus remains essentially passive. Momentum conservation then demands that the binary peak occurs exactly in the direction of \mathbf{q} . However, the binary peak can be shifted by contributions from higher-order mechanisms. More specifically, PCI effects tend to move the binary peak in the forward direction relative to \mathbf{q} [18,19,21,24,30]. Such a shift is also seen in the present data for those cases where the binary peak is resolved from the forward peak. Thus, signatures of strong PCI effects manifest themselves both in the forward and in the binary peak.

A surprising behavior is seen in the FDSC for $\varepsilon = 85$ eV. This energy loss corresponds to an electron to projectile speed ratio of $v_e/v_p = 1.22$, which cannot be regarded as falling within the velocity-matching regime. Therefore, one would expect the forward peak to be much less important relative to the binary peak than for the smaller energy losses. Indeed, the peak structure observed in the data for $\theta_p = 0.1$ mrad does not occur at $\theta_e = 0^\circ$, but rather close to the direction of \mathbf{q} ($\theta_q = 10^\circ$). Here, the forward peak is not resolved from the binary peak so that a quantitative evaluation of the contribution from

the forward peak is difficult. Nevertheless, the observation that the peak structure occurs very close to θ_q shows that the binary peak must be dominant. At $\theta_p = 0.2$ mrad the maximum has moved to even larger θ_e , and at 0° the FDSC is further reduced. However, at larger θ_p a sudden increase of the FDSC at 0° (relative to the value at θ_q) is seen. At $\theta_p = 0.3$ mrad a “shoulder” on the small-angle wing of the maximum is found and at $\theta_p = 0.5$ mrad a peak structure close to 0° clearly separated from the binary peak is observed. In fact, at this scattering angle the peak height ratio between the forward and binary peaks is quite similar to the corresponding values for the smaller energy losses. These data suggest that with increasing departure of the ejected electron speed from the projectile speed the relative importance of PCI tends to increase with increasing scattering angle, while for electron speeds equal to the projectile speed, within approximately 5%–10%, the opposite trend is observed. A similar conclusion was drawn for electrons well below the velocity-matching regime ejected in 16-MeV $O^{7+} + He$ collisions. There, an increasing forward shift of the binary peak with increasing q was found [38]. Later, such a trend was also theoretically predicted for fast proton-helium collisions [39]. However, at present we do not have a conceptual explanation for these trends.

The presence of separate forward and forward-shifted binary peak structures at $\theta_p = 0.5$ mrad may at first glance seem plausible. However, here, we point out that, in a classical picture, it is not straightforward to explain this phenomenon (and a classical explanation may not be possible at all). Both the existence of the forward peak and the forward shift of the binary peak are caused by the same mechanism, namely, by the attraction of the ejected electron toward the beam axis by the projectile. In both cases this attraction results in a shift of the corresponding peak relative to the direction of \mathbf{q} . The difference is merely of a quantitative nature: In the case of the forward peak this shift is equal to θ_q , while in the case of the binary peak it is only about 20%–30% of θ_q . This raises the question of why a shift of, say, 50% of θ_q is significantly less likely than a shift of 20%–30% and 100% of θ_q , i.e., why there is a minimum separating the forward and binary peaks. A resolution of this apparent dilemma is probably only possible within a quantum-mechanical treatment. There, the minimum can probably be interpreted as destructive interference between different transition amplitudes leading to the same final state.

The dashed blue curves in Figs. 1–4 represent our CDW-EIS calculations, which do not account for the PT interaction. The solid blue curves in Figs. 1–4 represent our CDW-EIS-PT calculations, which do account for the PT interaction [36]. The red curves show our 3DW-EIS calculations, which also account for the PT interaction [37]. As mentioned in the Introduction, CDW-EIS-PT and 3DW-EIS are conceptually very similar. The most important difference lies in the treatment of the PT interaction. While the CDW-EIS-PT model assumes straight-line trajectories, in the 3DW-EIS model the PT interaction is treated fully quantum mechanically.

The comparison between experiment and theory and between both theoretical models also reveals some similarities to the FDSC reported earlier for ionization of H_2 [24]. For the smallest and the largest energy losses, which are furthest

from the electron-projectile velocity matching, and at small θ_p , the 3DW-EIS calculations are in very good agreement with the experimental data. The CDW-EIS-PT calculations also reproduce the qualitative electron angular dependence of the measured FDCS very well, but there are considerable discrepancies in absolute magnitude. However, at large θ_p , especially for the other two energy losses close to the velocity matching, theory does not even reproduce the experimental data qualitatively. Furthermore, in spite of the conceptual similarities the two models differ substantially from each other in this regime. This reconfirms the conclusion, drawn from the fully differential study of ionization of H_2 , that the FDCS in the velocity-matching regime are particularly sensitive to the details of the few-body dynamics.

One important question is how PCI effects depend on the target ionization potential. By considering the asymptotic case of $I = 0$ one would expect such effects to become increasingly important with increasing I . This scenario is equivalent to the target nucleus not even being present. On the other hand, as mentioned in the Introduction, the interaction of the nucleus with either the ejected electron or the scattered projectile plays an essential role in PCI. One could argue that I approaching zero is not necessarily a signature of a vanishing nuclear charge, but that it can also signify an increasing screening of the nuclear charge by the passive electrons. However, the total unscreened charge of the nuclei is the same for H_2 and He. One would therefore expect the larger screened effective nuclear charge (which to a large extent determines I) of He, to lead to larger PCI effects than in H_2 . Instead, measured DDCS as a function of projectile energy loss and scattering angle seemed to suggest that PCI actually becomes stronger with decreasing I [16,27]. On the other hand, as mentioned in the Introduction, a follow-up study on DDCS for heavier targets [33] suggested that effects due to PCI could be masked by those due to another higher-order mechanism, involving the PT interaction, but only a single projectile-electron interaction (for simplicity, we refer to this process as the second-order PT process). Therefore, the dependence of PCI effects on I could not be conclusively determined from DDCS measurements.

Further insight should be obtainable from the FDCS measurements, especially by analyzing the forward peak. The second-order PT process is not expected to significantly contribute at $\theta_e = 0^\circ$ because there the last step in PCI, leading to the focusing toward 0° , is missing. Therefore, in contrast to DDCS, PCI effects to a large extent can be separated in the θ_e dependence of the FDCS from the second-order PT process. Considering the asymptotic case of I approaching 0 one would not only expect PCI to become weaker, but at the same time, the binary peak in the FDCS to become stronger and narrower. Therefore, if PCI effects indeed increase with increasing I , the ratio between the FDCS for ionization of He and H_2 should exhibit a strong maximum at $\theta_e = 0^\circ$. These ratios are shown in Fig. 5 for electrons emitted with the projectile speed (corresponding to $\varepsilon = 65.5$ eV for He and $\varepsilon = 57$ eV for H_2) and for $\theta_p = 0.1$ mrad (upper panel) and $\theta_p = 0.5$ mrad (lower panel) as a function of θ_e . At $\theta_p = 0.1$ mrad the ratios are essentially flat for $\theta_e > -30^\circ$. At $\theta_p = 0.5$ mrad, there appears to be a weak structure near $\theta_e = 45^\circ$, which is close to the direction of \mathbf{q} . Therefore, if there is any statistically significant departure from a flat dependence of R

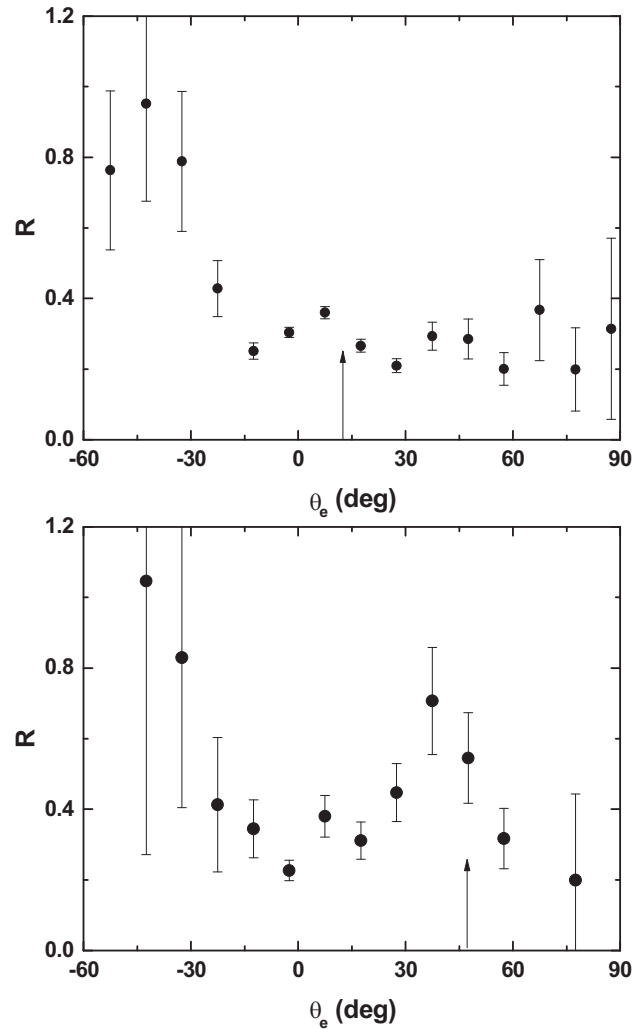


FIG. 5. Ratios between the fully differential cross sections for ionization of He and H_2 as a function of the electron ejection angle. For each target the electron energy corresponds to an electron speed equal to the projectile speed. The projectile scattering angle is fixed at 0.1 mrad (upper panel) and 0.5 mrad (lower panel).

on θ_e at all it would indicate a preference of the binary peak, rather than the forward peak, at larger I .

Apart from the forward peak in the electron angular distribution another prominent signature of PCI is a strong peak structure, the so-called cusp peak, in the electron energy spectrum at $E_e = \frac{1}{2}v_p^2$ (in a.u.) for θ_e fixed at 0° (see, e.g., [10,25,26]). If very small θ_p in addition to $\theta_e = 0^\circ$ are selected one would expect the cusp peak to become even more pronounced. In Fig. 6 the FDCS for $\theta_e = 0^\circ$ and for the same θ_p as in Figs. 1–4 (from upper left to lower right) are plotted as a function of E_e . Two remarkable features are seen in this figure: First, from the data the exact location of the cusp peak cannot be determined because of a large gap in the data between 5 and 38 eV; nevertheless it is clear that it occurs very close to, but slightly below $E_e = \frac{1}{2}v_p^2$ (indicated by the arrows). Second, a very steep high-energy wing of the cusp peak can even be seen at the largest scattering angle of 0.5 mrad. For comparison, in Fig. 7 the corresponding data are shown for ionization of H_2 .

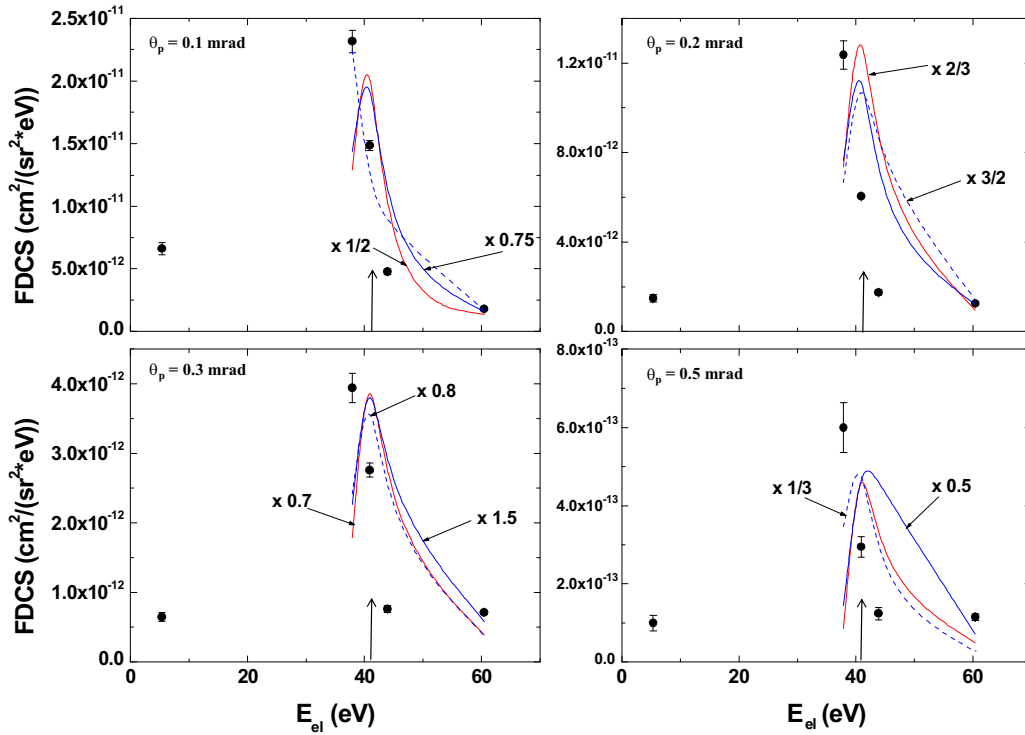


FIG. 6. Fully differential cross sections for electrons ejected into the scattering plane for a fixed electron ejection angle of 0° as a function of electron energy. The projectile scattering angles are indicated in the insets of each panel. Curves as in Figs. 1–4.

There, the cusp peak occurs exactly at $\frac{1}{2}v_p^2$ and it is only seen at the two smaller θ_p .

Both models accounting for the PT interaction predict the cusp peak very close to $E_e = \frac{1}{2}v_p^2$ for both targets (except

for the CDW-EIS-PT calculations at the largest scattering angle). However, interestingly the CDW-EIS calculation (not accounting for the PT interaction) agrees rather well with the experimental data for the He target at $\theta_p = 0.1$ mrad.

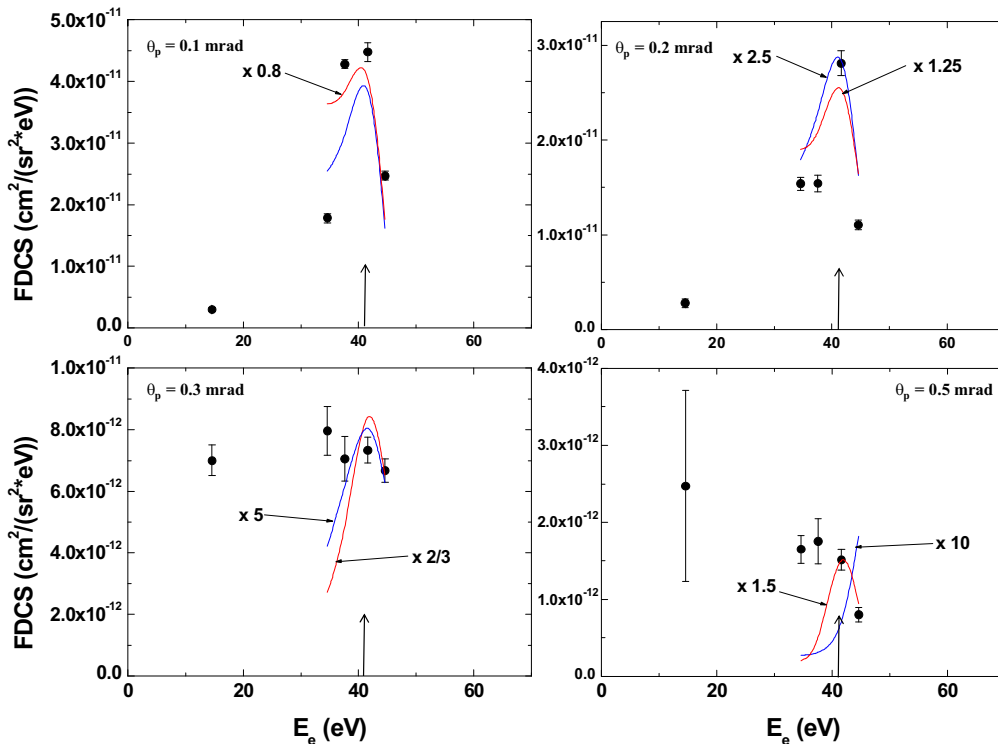


FIG. 7. Same as Fig. 6 for H_2 target; data and calculations from [24].

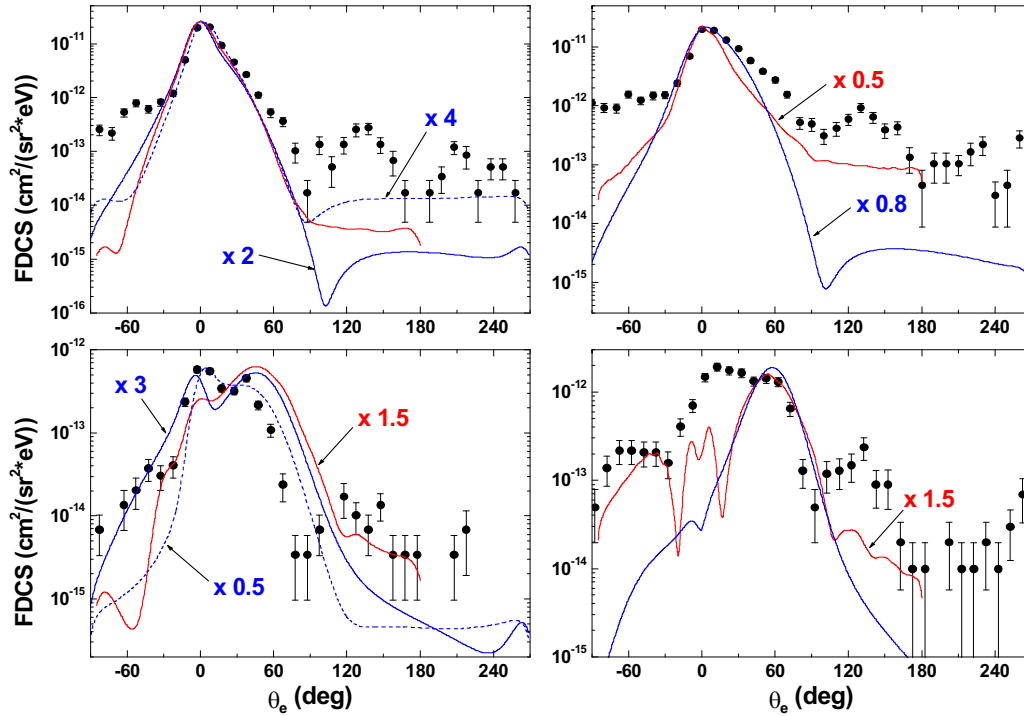


FIG. 8. Fully differential cross sections for electrons ejected from He (left panels) and H₂ (right panels) into the scattering plane for a projectile energy loss of 62.5 eV (He target) and 50 eV (H₂ target) as a function of the electron ejection angle. The projectile scattering angles are 0.1 mrad (upper panels) and 0.5 mrad (lower panels). Curves as in Figs. 1–4.

Furthermore, at $\theta_p = 0.5$ mrad the cusp peak is shifted to smaller E_e compared to the CDW-EIS-PT calculation. This can be taken as a hint that the shift of the cusp peak is characteristic to the $V_{pe}-V_{te}-V_{pe}$ interaction sequence. If this is indeed the case one would have to conclude that near the cusp energy PCI proceeds mostly through the $V_{pe}-V_{te}-V_{pe}$ sequence and that the $V_{pe}-V_{pt}-V_{pe}$ sequence is overestimated in the CDW-EIS-PT and 3DW-EIS models. Indications for such an overestimation were also found in the FDCS for ionization of H₂ [24] and in the DDCS for ionization of Ne and Ar [33].

The presence of a strong cusp peak even at large θ_p for He, but not for H₂, shows that the dependence of PCI effects on I changes with scattering angle. At small θ_p neither the electron angular distribution nor the electron energy dependence of the FDCS give any indication of an increasing role of PCI with increasing I , while at large θ_p PCI is clearly much more important for He than it is for H₂. In contrast, the CDW-EIS-PT and 3DW-EIS calculations yield strong cusp peaks for the H₂ target even at $\theta_p = 0.3$ mrad and the 3DW-EIS calculation also at $\theta_p = 0.5$ mrad. Furthermore, both calculations exhibit large differences to each other, especially at the largest θ_p . Therefore, the energy dependence of the FDCS, too, illustrates the high sensitivity of the cross sections to the few-body dynamics.

The ratios between the FDCS for ionization of He and H₂ plotted in Fig. 5 show a significant increase at negative electron emission angles. This suggests that apart from the forward and binary peaks additional structures may be present in the FDCS. To investigate this possibility further, we present the FDCS in Fig. 8 on a logarithmic scale for He at $\varepsilon = 62.5$ eV (left panels) and for H₂ at $\varepsilon = 50$ eV (right

panels). The scattering angle was fixed at $\theta_p = 0.1$ mrad (top panels) and $\theta_p = 0.5$ mrad (bottom panels). In order to reduce the statistical error bars, here the bin size in the electron angle was increased by a factor of 2. Indeed, especially at $\theta_p = 0.1$ mrad, a shoulder on the small-angle wing of the forward peak is visible for both targets. In addition, maxima are found near $\theta_e = 135^\circ$ and, in the case of the He target for $\theta_p = 0.1$ mrad, a weak peak near $\theta_e = 210^\circ$. The latter structure is not observed for larger θ_p and for the H₂ target at any θ_p .

The location of the structure around $\theta_e = 210^\circ$ coincides quite well with the direction of $-\mathbf{q}(\theta_{-q} \approx 195^\circ)$, where in a first-order treatment the recoil peak is expected. It is due to a direct hit between the projectile and the electron followed by a backscattering of the electron by its parent nucleus at 180° . Just like the binary peak, the recoil peak, too, is usually forward shifted relative to $-\mathbf{q}$ by PCI so that the location of the maximum in the data at 210° is consistent with the recoil peak. Furthermore, the absence of this structure for H₂ and at large θ_p is in accord with the expectation that the importance of the recoil peak (relative to the binary peak) decreases with increasing θ_p and decreasing I .

A structure at electron angles between 0° and -90° was also observed for ionization of He leading to $\varepsilon = 30$ eV [19]. It was interpreted within a classical picture as a two-step process, involving the PT interaction, in which the projectile passes the target atom between the nucleus and the active electron [40]. The interaction of the projectile with the electron leads to a forward component of the longitudinal momentum transfer. The interaction with the nucleus, in contrast, only transfers momentum in the transverse direction (because the

inelasticity in this interaction is practically zero). This interaction is on average stronger than the projectile-electron interaction so that the direction of the total transverse momentum transfer is opposite to the transverse electron momentum. This combination of a positive longitudinal and a negative transverse (relative to \mathbf{q}) electron momentum leads to an angle between 0° and -90° . The electrons emitted in this region were labeled “swing by electrons” [40].

In contrast to the recoil peak and swing by electron “shoulder,” a structure analogous to the one found in the present data around $\theta_e \approx 135^\circ$ was not reported in previous publications on FDCS measurements, which were all performed for electron energies well below the velocity-matching regime. It seems plausible to attempt to understand the origin of this peak by comparing to theoretical models. However, the sensitivity of the FDCS to the details of the few-body dynamics, which is normally regarded as a benefit, could become a problem if it is too high and if the primary goal is to identify the mechanism leading to a specific feature in the data. In this case, it can be very difficult to identify any systematic trend in the agreement (or lack thereof) with the data depending on the theoretical description of certain physical effects. This is illustrated in the following comparison between the data and the CDW-EIS-PT and 3DW-EIS models in the region of the structures which are too small to be visible on a linear scale.

Overall, the agreement between experiment and theory outside the regions of the forward and binary peaks is not good. On the other hand, there is an element of qualitative agreement insofar as under certain kinematic conditions one or both theoretical models show the features seen in the data approximately in the same region. For example, at $\theta_p = 0.1$ mrad the CDW-EIS-PT calculations shows a minimum at about $\theta_e = 100^\circ$ for both targets, which in the experimental data separates the binary peak (not resolved from the forward peak) from the structure around 135° . Furthermore, in the 3DW-EIS calculations a maximum can be seen in the region of the swing by electrons, which is even in reasonably good quantitative agreement with the data at $\theta_p = 0.5$ mrad in the case of the H_2 target. Furthermore, some structures are visible in the same calculation in the region of the maximum around 135° . However, given the large overall discrepancies it is not clear how significant this qualitative agreement is. Furthermore, it is difficult to discern a systematic pattern under which condition a particular model reproduces the data better or worse than the others. For example, in the swing by electron region at $\theta_p = 0.5$ mrad the 3DW-EIS model reproduces the data for the H_2 fairly well, while the CDW-EIS-PT model is in poor agreement, but for the He target the roles are reversed and the CDW-EIS-PT model reproduces the data much better than the 3DW-EIS model. At $\theta_p = 0.1$ mrad both models are in poor agreement with the data for both targets. Furthermore, it is difficult to evaluate the role of the PT interaction. Comparing the CDW-EIS, CDW-EIS-PT, and 3DW-EIS calculations to the data for the He target at $\theta_p = 0.5$ mrad, one might be tempted to conclude that the 135° structure is caused by a mechanism involving the PT interaction because both models including this interaction are significantly closer to the experimental data. However, at $\theta_p = 0.1$ mrad for the same target, the CDW-EIS results are in much better agreement.

The discussion above suggests that identifying the mechanisms underlying the various structures in the FDCS requires having theoretical models which yield better overall agreement with the experimental data. Both approaches presented here are perturbative distorted wave methods, for which the range of validity is crudely given by the condition $Q_p/v_p^2 \ll 1$ [41], which is marginally satisfied for the collision system studied here ($Q_p/v_p^2 = 0.33$). A perhaps even bigger problem is that the capture channel is not included. This channel is expected to have a particularly large effect on FDCS for ionization in the velocity-matching regime because of the energetic proximity of the final electron continuum state to the bound states in the projectile. In spite of these constraints the CDW-EIS-PT and 3DW-EIS models were quite successful in reproducing experimental data for electron energies well below the velocity-matching regime [19,32]. The present data show the limitations of perturbative approaches and demonstrate that calculating FDCS for electrons in the cusp peak is one of the biggest remaining challenges in advancing our understanding of the few-body dynamics underlying ionization.

Nonperturbative approaches for ion impact are much more challenging to implement than for electron impact, because the much larger projectile mass means that a much larger number of angular momentum states have to be considered for the scattered projectiles. Nevertheless, in recent years such models were developed to describe ionization by ion impact (see, e.g., [30,42,43]). They use basis sets including projectile states so that the capture channel is accounted for. Two of these models [30,42] were used to calculate DDCS and one [30] to calculate FDCS for ionization of atomic hydrogen. There, the FDCS at the matching velocity look qualitatively quite similar to the present data for ionization of He. Furthermore, the DDCS are in good agreement with experimental data [27,44]. More recently, one model [42] was applied to calculate FDCS for ionization of He for electron energies well below the velocity-matching regime [45]. Improved agreement with the experimental data, compared to perturbative approaches, was achieved. These are promising indicators that comparison of measured FDCS in the velocity-matching regime to nonperturbative calculations will result in a major advancement in the understanding of the few-body dynamics underlying ionization.

V. CONCLUSIONS

We have measured and calculated fully differential cross sections (FDCS) for ionization of helium by 75-keV proton impact for electrons ejected with a speed close to the projectile speed. Apart from the binary peak, occurring near the direction of the momentum transfer \mathbf{q} , which usually dominates the FDCS for relatively small electron energies, we also observe a strong peak structure in the forward direction. This forward peak is a manifestation of a higher-order process, known as postcollision interaction (PCI), which involves two (or more) interactions between the projectile and the active electron and an additional interaction of the target nucleus with either the projectile or the electron.

The data were compared to those previously published for ionization of H_2 . In the electron angle dependence of the FDCS for fixed projectile scattering angle and electron

energy we did not find any signatures suggesting that PCI was more important for one target than for the other. However, in the electron energy dependence of the FDCS for an electron ejection angle fixed at $\theta_e = 0$ and projectile scattering angles fixed at large values, PCI leads to a much more pronounced cusp peak for He than it does for H₂. This trend is not reproduced by theory.

While for small electron energies perturbative distorted wave approaches often yield satisfactory agreement with experimental data, major discrepancies are found in the present data taken in the velocity-matching regime. Furthermore, two conceptually very similar versions of such distorted wave approaches differ significantly from each other. This confirms a very high sensitivity of the FDCS to the details of the underlying few-body dynamics in the velocity-matching regime found earlier for ionization of H₂. In fact, the level of sensitivity is so high that it actually turns into a detriment: The resulting discrepancies among different theories and with experimental data seem to lack any systematic pattern that could be used to track the physics underlying the observed

features in the FDCS or which is missing (or not sufficiently accounted for) in theory.

A further complication for perturbative methods is presented by the sensitivity of FDCS to the projectile coherence properties [46,47]. Along with the other constraints discussed in this article this suggests that a time-dependent, nonperturbative calculation, using a large two-center basis set and describing the projectiles by a wave packet with a width reflecting the coherence length, would have a high potential for providing important insight into the understanding of the measured FDCS even in the velocity-matching regime.

ACKNOWLEDGMENTS

This work was supported by the National Science Foundation under Grants No. PHY-1703109 and No. PHY-1505819. M.F.C. acknowledges support from the project “Advanced research using high intensity laser produced photons and particles” (CZ.02.1.01/0.0/0.0/16 019/0000789) from the European Regional Development Fund (ADONIS).

-
- [1] M. E. Rudd, Y.-K. Kim, D. H. Madison, and J. W. Gallagher, *Rev. Mod. Phys.* **57**, 965 (1985).
- [2] N. Stolterfoht, R. D. DuBois, and R. D. Rivarola, *Electron Emission in Heavy Ion-Atom Collisions* (Springer Verlag, Heidelberg, 1997).
- [3] M. E. Rudd, Y.-K. Kim, D. H. Madison, and T. J. Gay, *Rev. Mod. Phys.* **64**, 441 (1992).
- [4] M. Schulz and D. H. Madison, *Int. J. Mod. Phys. A* **21**, 3649 (2006).
- [5] M. E. Rudd and T. Jorgensen, *Phys. Rev.* **131**, 666 (1963).
- [6] V. V. Afrosimov, Yu. A. Mamaev, M. N. Panov, and V. Uroshevich, *Zh. Tekh. Fiz.* **37**, 717 (1967) [*Sov. Phys. - Tech. Phys.* **12**, 512 (1967)].
- [7] J. T. Park, J. E. Aldag, J. M. George, J. L. Peacher, and J. H. McGuire, *Phys. Rev. A* **15**, 508 (1977).
- [8] M. B. Shah and H. B. Gilbody, *J. Phys. B* **14**, 2361 (1981).
- [9] M. E. Rudd, R. D. DuBois, L. H. Toburen, C. A. Ratcliffe, and T. V. Goffe, *Phys. Rev. A* **28**, 3244 (1983).
- [10] G. B. Crooks and M. E. Rudd, *Phys. Rev. Lett.* **25**, 1599 (1970).
- [11] D. H. Lee, P. Richard, T. J. M. Zouros, J. M. Sanders, J. L. Shinpaugh, and H. Hidmi, *Phys. Rev. A* **41**, 4816 (1990).
- [12] L. C. Tribedi, P. Richard, D. Ling, Y. D. Wang, C. D. Lin, R. Moshhammer, G. W. Kerby, M. W. Gealy, and M. E. Rudd, *Phys. Rev. A* **54**, 2154 (1996).
- [13] R. Schuch, H. Schöne, P. D. Miller, H. F. Krause, P. F. Dittner, S. Datz, and R. E. Olson, *Phys. Rev. Lett.* **60**, 925 (1988).
- [14] H. Schöne, R. Schuch, S. Datz, M. Schulz, P. F. Dittner, J. P. Giese, Q. C. Kessel, H. F. Krause, P. D. Miller, and C. R. Vane, *Phys. Rev. A* **51**, 324 (1995).
- [15] E. Y. Kamber, C. L. Cocke, S. Cheng, and S. L. Varghese, *Phys. Rev. Lett.* **60**, 2026 (1988).
- [16] T. Vajnai, A. D. Gaus, J. A. Brand, W. Htwe, D. H. Madison, R. E. Olson, J. L. Peacher, and M. Schulz, *Phys. Rev. Lett.* **74**, 3588 (1995).
- [17] M. Schulz, R. Moshhammer, D. Fischer, H. Kollmus, D. H. Madison, S. Jones, and J. Ullrich, *Nature* **422**, 48 (2003).
- [18] D. Fischer, R. Moshhammer, M. Schulz, A. Voitkiv, and J. Ullrich, *J. Phys. B* **36**, 3555 (2003).
- [19] N. V. Maydanyuk, A. Hasan, M. Foster, B. Tooke, E. Nanni, D. H. Madison, and M. Schulz, *Phys. Rev. Lett.* **94**, 243201 (2005).
- [20] H. Gassert, O. Chuluunbaatar, M. Waitz, F. Trinter, H.-K. Kim, T. Bauer, A. Laucke, Ch. Müller, J. Voigtsberger, M. Weller, J. Rist, M. Pitzer, S. Zeller, T. Jahnke, L. P. H. Schmidt, J. B. Williams, S. A. Zaytsev, A. A. Bulychev, K. A. Kouzakov, H. Schmidt-Böcking *et al.*, *Phys. Rev. Lett.* **116**, 073201 (2016).
- [21] O. Chuluunbaatar, K. A. Kouzakov, S. A. Zaytsev, A. S. Zaytsev, V. L. Shablov, Yu. V. Popov, H. Gassert, M. Waitz, H.-K. Kim, T. Bauer, A. Laucke, C. Müller, J. Voigtsberger, M. Weller, J. Rist, K. Pahl, M. Honig, M. Pitzer, S. Zeller, T. Jahnke *et al.*, *Phys. Rev. A* **99**, 062711 (2019).
- [22] R. Dörner, V. Mergel, O. Jagutzski, L. Spielberger, J. Ullrich, R. Moshhammer, and H. Schmidt-Böcking, *Phys. Rep.* **330**, 95 (2000).
- [23] J. Ullrich, R. Moshhammer, A. Dorn, R. Dörner, L. Schmidt, and H. Schmidt-Böcking, *Rep. Prog. Phys.* **66**, 1463 (2003).
- [24] M. Dhital, S. Bastola, A. Silvas, A. Hasan, B. R. Lamichhane, E. Ali, M. F. Ciappina, R. A. Lomsadze, D. Cikota, B. Boggs, D. H. Madison, and M. Schulz, *Phys. Rev. A* **99**, 062710 (2019).
- [25] L. Sarkadi, J. Palinkas, A. Köver, D. Berenyi, and T. Vajnai, *Phys. Rev. Lett.* **62**, 527 (1989).
- [26] L. C. Tribedi, P. Richard, Y. D. Wang, C. D. Lin, L. Gulyas, and M. E. Rudd, *Phys. Rev. A* **58**, 3619 (1998).
- [27] M. Schulz, A. C. Laforge, K. N. Egodapitiya, J. S. Alexander, A. Hasan, M. F. Ciappina, A. C. Roy, R. Dey, A. Samolov, and A. L. Godunov, *Phys. Rev. A* **81**, 052705 (2010).
- [28] L. Sarkadi, L. Gulyas, and L. Lugosi, *Phys. Rev. A* **65**, 052715 (2002).
- [29] U. Chowdhury, M. Schulz, and D. H. Madison, *Phys. Rev. A* **83**, 032712 (2011).

- [30] H. R. J. Walters and C. T. Whelan, *Phys. Rev. A* **92**, 062712 (2015).
- [31] A. Hasan, S. Sharma, T. P. Arthanayaka, B. R. Lamichhane, J. Remolina, S. Akula, D. H. Madison, and M. Schulz, *J. Phys. B* **47**, 215201 (2014).
- [32] M. F. Ciappina, C. A. Tachino, R. D. Rivarola, S. Sharma, and M. Schulz, *J. Phys. B* **48**, 115204 (2015).
- [33] A. Silvus, M. Dhital, S. Bastola, J. Buxton, Z. Klok, E. Ali, M. F. Ciappina, B. Boggs, D. Cikota, D. H. Madison, and M. Schulz, *J. Phys. B* **52**, 125202 (2019).
- [34] M. Schulz, in *Advances in Atomic, Molecular, and Optical Physics*, edited by S. Yelin, E. Arimondo, and C. C. Lin (Elsevier, Amsterdam, 2017), Vol. 66, pp. 508–543.
- [35] A. D. Gaus, W. Htwe, J. A. Brand, T. J. Gay, and M. Schulz, *Rev. Sci. Instrum.* **65**, 3739 (1994).
- [36] M. F. Ciappina, W. R. Cravero, and M. Schulz, *J. Phys. B* **40**, 2577 (2007).
- [37] M. Foster, J. L. Peacher, M. Schulz, A. Hasan, and D. H. Madison, *Phys. Rev. A* **72**, 062708 (2005).
- [38] M. Schulz, B. Najjari, A. B. Voitkiv, K. Schneider, X. Wang, A. C. Laforge, R. Hubele, J. Goullon, N. Ferreira, A. Kelkar, M. Grieser, R. Moshhammer, J. Ullrich, and D. Fischer, *Phys. Rev. A* **88**, 022704 (2013).
- [39] O. Chuluunbaatar, S. A. Zaytsev, K. A. Kouzakov, A. Galstyan, V. L. Shablov, and Yu. V. Popov, *Phys. Rev. A* **96**, 042716 (2017).
- [40] J. Fiol and R. E. Olson, *J. Phys. B* **35**, 1759 (2002).
- [41] D. S. F. Crothers and J. F. McCann, *J. Phys. B* **16**, 3229 (1983).
- [42] I. B. Abdurakhmanov, J. J. Bailey, A. S. Kadyrov, and I. Bray, *Phys. Rev. A* **97**, 032707 (2018).
- [43] M. S. Pindzola, J. Colgan, Robicheaux, T. G. Lee, M. F. Ciappina, M. Foster, J. A. Ludlow, and S. A. Abdel-Naby, *Adv. At., Mol. Opt. Phys.* **65**, 291 (2016).
- [44] A. C. Laforge, K. N. Egodapitiya, J. S. Alexander, A. Hasan, M. F. Ciappina, M. A. Khakoo, and M. Schulz, *Phys. Rev. Lett.* **103**, 053201 (2009).
- [45] S. U. Alladustov, I. B. Abdurakhmanov, A. S. Kadyrov, I. Bray, and K. Bartschat, *J. Phys.: Conf. Ser.* (unpublished).
- [46] K. N. Egodapitiya, S. Sharma, A. Hasan, A. C. Laforge, D. H. Madison, R. Moshhammer, and M. Schulz, *Phys. Rev. Lett.* **106**, 153202 (2011).
- [47] L. Nagy, F. Jarai-Szabo, S. Borbely, T. Arthanayaka, B. R. Lamichhane, A. Hasan, and M. Schulz, in *Interdisciplinary Research on Particle Collisions and Quantitative Spectroscopy*, edited by Dz. Belkic (World Scientific Publishing, Singapore) (unpublished).